Nanoscale

Accepted Manuscript

This article can be cited before page numbers have been issued, to do this please use: T. J. Scarborough, Y. Kawai-Harada, O. Brennan, C. Chan, M. Harada and S. P. Walton, *Nanoscale*, 2026, DOI: 10.1039/D6NR01765G.

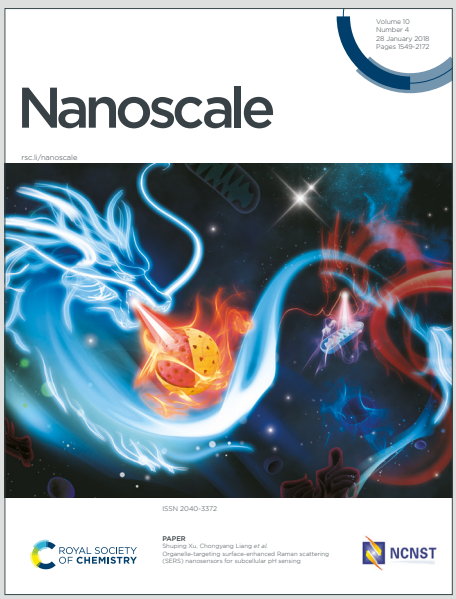

ROYAL SOCIETY OF CHEMISTRY

rsc.li/nanoscale

View Article Online
DOI: 10.1039/D6NR01765G

Tangential flow filtration for isolating exomeres and other nanoscale extracellular particles

Thomas Scarborough,[1] Yuki Kawai-Harada,[2,3] Olivia Brennan,[1] Christina Chan,[1,2,3] Masako Harada,[2,3]* S. Patrick Walton[1]*

[1]Department of Chemical Engineering and Materials Science, Michigan State University, East Lansing, Michigan

[2]Department of Biomedical Engineering, Michigan State University, East Lansing, Michigan

[3]Institute for Quantitative Health Science and Engineering (IQ), Michigan State University, East Lansing, Michigan

*Corresponding Authors

Abstract

Extracellular particles, including extracellular vesicles (EVs) and non-vesicular extracellular particles (NVEPs), enable intercellular communication by transferring regulatory miRNAs and other biomolecules. While EVs have been studied for drug delivery, NVEPs remain relatively unexplored. Exomeres, a recently discovered class of NVEPs enriched in RNAi proteins, preferentially carry miRNAs and deliver them to cells more effectively than EVs, underscoring their potential as vehicles for therapeutic RNAs. One current limitation to studying and applying exomeres for therapeutic RNA delivery is the lack of scalable, cost-effective, and rapid isolation methods. Here, we investigated whether tangential flow filtration (TFF), a common bioseparation approach that separates species by size, would effectively isolate exomeres from conditioned media with comparable purity and identity to exomeres isolated by differential ultracentrifugation. TFF successfully isolated exomeres that were enriched in RNAi components including Argonaute-2 (AGO2), heat shock protein (HSP)90AB1, and a unique set of miRNAs not abundant in EVs. Remarkably, exomere-encapsulated miRNAs were resistant to nuclease degradation even after treatment with protease and surfactant, suggesting that exomeres are highly stable, non-vesicular complexes with potentially extended circulating half-lives. Together, our results establish TFF as an efficient bench-scale method for isolating exomeres, and further demonstrate that TFF could potentially be applied in a bioprocess for exomere-based RNA therapeutic production. This study is also the first to demonstrate that exomere miRNAs are highly resistant to nuclease degradation,

View Article Online
DOI: 10.1039/D6NR01765G

suggesting that exomeres could complement and potentially outperform current clinical standards for RNA delivery.

Keywords

Exomeres, extracellular particles, RNA therapeutics, tangential flow filtration

Introduction

It is now well-established that intercellular communication is mediated by a variety of extracellular particles (EPs), including extracellular vesicles (EVs) and non-vesicular extracellular particles (NVEPs), that transfer a broad range of biomolecules from donor to recipient cells.[1] Detailed characterization of the biogenesis, release, and uptake of EVs – membranous EPs generated by plasma membrane budding or from intraluminal vesicles of the endosome[2] – has already demonstrated proof of concept for EP-mediated delivery of therapeutic RNAs. For example, surface-engineered exosomes loaded with siRNAs repress BACE1 in brain cells, miR-140-loaded exosomes slow the progression of osteoarthritis by targeting chondrocytes, and microvesicles carrying TGF-β1 siRNAs increase apoptosis and reduce migration in sarcoma cells.[3–5]

The recent discovery of exomeres, a non-vesicular subclass of EPs, revealed yet another specialized cell messenger implicated in intercellular transfer of RNA and other biomolecules.[6–8] Exomeres are ~35-50 nm protein-rich complexes that are naturally enriched in miRNAs and proteins related to RNA interference (RNAi).[6,7,9] Two unique features of exomeres suggest that they have considerable potential for use in RNAi therapeutics. First, Argonaute-2 (AGO2) preferentially associates with exomeres as compared to EVs.[6,7] In human plasma, the majority of miRNAs purify with non-vesicular AGO2-containing complexes.[10] Second, miRNAs occupy a substantially higher proportion of the total RNA content in exomeres versus other EP types.[7] These observations suggest that i) the primary functional role of exomeres may be to activate RNAi in recipient cells, and ii) in the absence of a protective lipid bilayer, exomeres are sufficiently stable to deliver intact miRNAs to recipient cells. Indeed, it has already been shown that trophoblast-derived exomeres deliver miR-517a-3p to Jurkat cells more effectively than EVs.[8] Together, these

View Article Online
DOI: 10.1039/D6NR01765G

attributes make it important to investigate exomeres as a potential delivery platform for the next-generation of RNAi-based therapeutics.

Careful study of exomeres requires reproducible isolation of a sufficiently pure particle population at reasonable scale. At present, separation of exomeres from other EPs remains a substantial challenge. Asymmetric flow field-flow fractionation (AF4), the technique used to initially discover exomeres, can isolate relatively pure populations but requires fine-tuning for each application.[9,11] An alternative protocol using differential ultracentrifugation (UC) was later introduced, but is time-intensive and cannot readily be scaled up to meet the demands of an industrial bioprocess.[12] Moreover, UC can exert significant shear forces on particles, causing fragmentation and making it difficult to determine whether the recovered material accurately reflects what was originally produced by cells.[13] Most recently, a fast protein liquid chromatography size-exclusion chromatography (FPLC-SEC) approach was developed to address some of the limitations of UC. FPLC-SEC is more scalable than UC and can be operated at high flow rates and under modest pressures.[14,15] SEC has already been used in biomanufacturing contexts, such as for assessing recombinant protein aggregation.[16] However, large column volumes (CV) can constrain fractionation-based processes (i.e., when fractionation is used as a primary means of particle separation) because the feed volume is limited to ~2-6% of the CV.[17] There remains a significant need for an approach for exomere isolation that is cost-effective, scalable when used as the primary means for exomere isolation (e.g., as in an industrial bioprocess), and able to yield highly pure populations with minimal processing stress.

Tangential flow filtration (TFF) is a form of ultrafiltration that separates particles based on differences in their hydrodynamic characteristics. TFF systems are relatively straightforward to design, highly cost-effective when combined with membrane cleaning and reuse, and not dependent on specialized equipment.[18] Because TFF membrane pore sizes can be tuned to the specific application, TFF has already been used to isolate a wide range of biological species at the bench-scale including EVs, plasmid DNA nanoparticles, and viruses.[19–22] TFF also has broad translational potential. A cGMP-compatible process comprised of hollow fiber bioreactor cell

View Article Online
DOI: 10.1039/D6NR01765G

culture, TFF, and SEC was recently introduced to isolate IL-15 cytokine-enriched EVs for oncotherapy. Using a pump-driven, isovolumetric TFF system outfitted with a 0.05 μm hollow fiber polysulfone membrane, biologically active EVs were purified from more than 200 mL of conditioned media.[23] In viral vaccine manufacturing, in-line TFF with a 100 kDa hollow fiber cartridge was used to purify and concentrate Vero cell-producing recombinant vesicular stomatitis virus (rVSV) from 1.6 L of media down to 750 mL with no loss in viral titer (1.03×10^{12} pfu/mL to 2.47×10^{12} pfu/mL).[24] TFF combined with other bioprocesses has become a common approach for improving yield and purity of biologics. For example, TFF-SEC was used to process up to six liters of mesenchymal stromal cell culture medium to isolate and purify immunosuppressive EVs.[25] Others have developed automated technologies that integrate TFF and centrifugation to isolate EVs from up to 10 liters of cell culture supernatant.[26]

When considering drug product commercialization, one significant benefit of TFF over other nanoparticle purification methods is the ability to employ the same process design at each phase of product development. Because the volume of processable material scales proportionally to membrane surface area[18], a single TFF process with an appropriate scaling factor can be employed at the bench, in pilot studies, and in commercial manufacturing. A complete scale-up for Lumefantrine nanoparticles to treat malaria was recently published and employed TFF for concentration. Shear rates and transmembrane pressures were optimized on a single lumen lab-scale filtration module and translated to a 19 lumen industrial system operating at 5 L min^{-1} for 360 L batches.[27]

Given the versatility and clear translational potential of TFF as a purification scheme for biologics, we sought to develop a proof of concept, bench-scale tandem TFF method to isolate EVs and exomeres from the conditioned media of HEK293T cells (**Fig. 1**). The objectives of our study were to: (1) develop a bench-scale tandem TFF protocol for exomere isolation, (2) compare the

View Article Online
DOI: 10.1039/D6NR01765G

purity and yield of TFF-isolated particles to particles isolated by ultracentrifugation, and (3) characterize the physical and molecular properties of TFF-isolated exomeres.

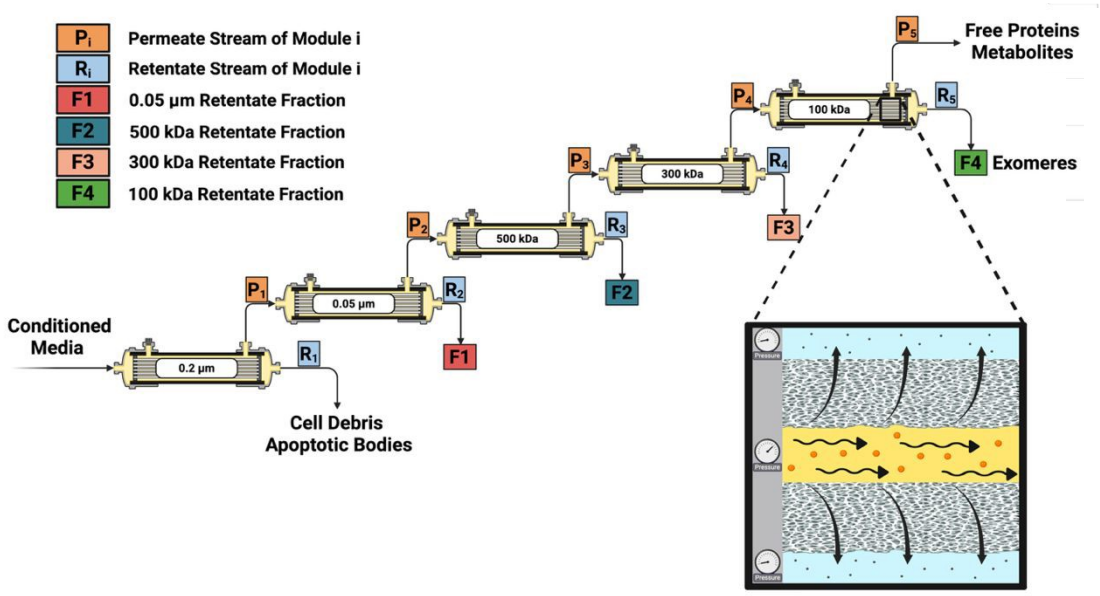

Figure 1: Bench-scale tandem TFF for isolating exomeres and other extracellular particles from conditioned media. Particle separation is driven by a pressure differential across a semiporous membrane. Conditioned media is first fed to a 0.2 μm clarifying filter to remove cell debris and apoptotic bodies. The permeate is collected and delivered to the next filter in the series. Retained particles on membranes F1-F4 are diafiltered with HEPES-supplemented PBS before collection. Figure created with BioRender.com.

Experimental Methods

Cell culture. HEK293T cells (ATCC, CRL-3216) were seeded in high glucose DMEM supplemented with 10% (v/v) FBS and 100 units/mL Penicillin-Streptomycin at a density of 10,000 cells/cm^2 in 10 cm dishes (small scale) or 18,500 cells/cm^2 in T225 vented flasks (large scale, optimized conditions) and incubated at 37°C, 5% CO_2 until the cells were approximately 50-60% confluent. Cells were washed with PBS 3 times then changed to serum-free DMEM (Thermo, 31053028) supplemented with 100 units/mL Penicillin-Streptomycin, 4 mM L-Glutamine, and 1X Insulin-Transferrin-Selenium (ITS) (Corning, 25-800-CR) for conditioned media production. Conditioned media was collected when cells reached 80-90% confluence and processed by TFF the same day.

View Article Online
DOI: 10.1039/D6NR01765G

Whole cell lysate isolation. Cells were trypsinized and pelleted at 300 x g for 3 minutes. After removal of the supernatant, cells were resuspended in 1 mL of PBS followed by centrifugation at 300 x g for an additional 3 minutes. The supernatant was removed followed by pellet resuspension in 1 mL of ice-cold RIPA buffer supplemented with EDTA-free Halt™ protease inhibitor cocktail (Thermo, 78425). After briefly vortexing, homogenates were placed on ice for 30 minutes followed by centrifugation for 15 minutes at 14,000 x g, 4°C to clear the lysates. Supernatants were collected and stored at 4°C for a maximum of 1 week or -80°C long-term.

EP isolation by bench-scale tandem TFF (Fig. 1). Five MicroKros (small scale) or MidiKros (large scale) hollow fiber membranes of sizes and membrane material: 0.2 μm (polyethersulfone, PES), 0.05 μm - F1 (polysulfone, PS), 500 kDa MWCO - F2 (modified polyethersulfone, mPES), 300 kDa MWCO - F3 (mPES), and 100 kDa MWCO - F4 (mPES) (Spectrum®, Repligen) were preconditioned with DI water followed by PBS containing 25 mM HEPES solution (Sigma-Aldrich, H0887), termed PBS-H.[12] Preconditioning solutions were used at a volume of 2 mL/cm^2 membrane surface area. Each TFF module was operated manually using the various configurations depicted in **Supp. Fig. 1**. Conditioned media was first clarified with a 0.2 μm filter to remove cell debris and apoptotic bodies. The permeate was collected and fed to the remaining 4 filters sequentially. The retentate of the 0.2 μm filter and permeate of the 100 kDa filter were discarded.

For particle isolation, retained particles in each module (1-4 mL particle suspension depending on scale) were diafiltered with 8-10 diavolumes of 25 mM PBS-H to remove free proteins and exchange buffers. Fluid volumes were reduced to 1 mL for MicroKros filters or 2-3 mL for MidiKros filters before manual collection via syringe. Except for those used in RNase protection assays and SEC, particle suspensions were immediately supplemented with EDTA-free protease inhibitor cocktail, inverted briefly to mix, and stored at 4°C until use. Samples were stored at -80°C if not used within 1 week. Each fraction was designated F1-F4, with smaller numbers corresponding to larger membrane pore sizes.

To regenerate TFF membranes, modules were flushed immediately after use with 2 mL/cm^2 DI water, followed by 15 mL of 0.5 M NaOH, and then stored in 0.1 M NaOH at 4°C until

View Article Online
DOI: 10.1039/D6NR01765G

the next use. Modules were replaced in their entirety when protein content for a given fraction significantly changed, or substantial EV contamination of the non-vesicular fractions was noticed in routine assays. No visible fouling of the hollow fibers was observed after operation or cleaning. Typically, filters were used for 5 to 7 isolations before replacement.

Size Exclusion Chromatography (SEC). Gravity-flow SEC was carried out on TFF fractions using qEVoriginal 20 nm columns (IZON, ICO-20) following the manufacturer's instructions. Briefly, columns were flushed with 2 column volumes of degassed PBS (Thermo, 10010-023) before the addition of 500 μL of TFF F2 (EVs) or F4 (exomeres). 21 fractions of 400 μL each were collected after the elution of 2 mL of buffer (void) volume. Columns were flushed with 8.5 mL of 0.5 M NaOH followed by 17 mL of PBS before addition of the next sample and were reused no more than 4 times.

Dot Blot. 400 μL SEC fractions were dotted onto dry 0.45 μm nitrocellulose membranes (Whatman, Protran BA 85) using a 96-well S&S minifold® I vacuum manifold system and left to dry overnight at room temperature (RT). The next morning, membranes were blocked in EveryBlot blocking buffer (Bio-Rad, 12010020) for 1 hour at RT with gentle rocking. Primary antibodies were diluted (1:1000) in blocking buffer and incubated with the blots for 1.5 hours at RT with gentle rocking. After incubation, blots were washed with TBST 3 times for 5 minutes each. The secondary antibody was diluted (1:20000) in blocking buffer and incubated with the blots for 1 hour at RT with gentle rocking. After incubation, blots were again washed with TBST 3 times for 5 minutes each. Chemiluminescent signals were developed with SuperSignal™ West Pico PLUS substrate (Thermo, 34580) for 5 minutes before imaging on a Bio-Rad Chemidoc system. The following primary antibodies were used: rabbit anti-AGO2 (Abcam, ab186733), rabbit anti-CD9 (Abcam, ab236630), rabbit anti-LGALS3BP (Proteintech, 10281-1-AP). The following secondary antibody was used: goat anti-rabbit IgG, HRP-conjugated (Thermo, 31460). For AGO2 detection in the TFF F4 exomere fraction, 50 mM DTT (Bio-Rad, 1610611) was added to each SEC fraction and samples heated at 95°C for 5 minutes before dotting. Dot blots were uniformly processed in ImageJ 1.54g (Java 1.8.0_345) using brightness adjustment to better visualize weak signals.

View Article Online
DOI: 10.1039/D6NR01765G

EP isolation by differential ultracentrifugation (UC). Differential UC was carried out in the manner previously described.[12] Briefly, conditioned media was centrifuged for 10 minutes at 500 x g, 4°C to remove cell debris, followed by centrifugation of the supernatant for 20 minutes at 2,000 x g, 4°C to remove apoptotic bodies. The resulting supernatant was centrifuged for 40 minutes at 10,000 x g, 4°C to obtain crude large EVs (LEVs) as a pellet. The pellet was resuspended in PBS-H and washed by an additional centrifugation cycle at 10,000 x g, 4°C. The LEV supernatant was clarified using a 0.2 μm filter, then concentrated with a 100 kDa MWCO centrifugal concentrator (Millipore, UFC710008). Small EVs (sEVs) were isolated by ultracentrifugation of the concentrate. The concentrate was first diluted to 37 mL with PBS-H then centrifuged at 167,000 x g for 4 hours, 4°C in a Beckman Coulter SW 32 Ti swinging-bucket rotor. The crude sEV pellet was washed by suspension of the pellet in 37 mL PBS-H followed by centrifugation at 167,000 x g, 4°C for 4 hours. To isolate exomeres, the sEV supernatant was centrifuged at 167,000 x g, 4°C for 16 hours, resuspended in 37 mL of PBS-H, then washed by centrifugation at 167,000 x g, 4°C for an additional 16 hours. Resuspended particles were stored at 4°C for a maximum of 1 week or at -80°C for longer periods.

Protein quantification. EP samples were quantified without prior lysis. Protein content was estimated using the Pierce™ BCA protein assay (Thermo, 23225) following the manufacturer's instructions for the microplate procedure, modifying the protocol to increase the incubation time to 2 hours from 30 minutes.

SDS-PAGE and Western blot. Samples were mixed with 4X Laemmli buffer (Bio-Rad, 1610747) at a ratio of 3:1 (v/v) with or without 50 mM DTT depending on the antigen, then denatured at 95°C for 5 minutes. For SDS-PAGE, 2.5-10 μg of total protein was loaded per lane onto 4-20% precast polyacrylamide gels (Bio-Rad, 4561094) and separated at 200 volts for approximately 35 minutes. Equal amounts of protein were loaded per lane. Proteins were transferred to 0.2 μm PVDF membranes (Bio-Rad, 1704156) using a Trans-Blot Turbo system with the mixed molecular weight protocol (25 V, 1.3 A, 7 minutes). After transfer, blots were blocked with EveryBlot blocking buffer

View Article Online
DOI: 10.1039/D6NR01765G

for 1 hour at RT with agitation, followed by primary antibody incubation for 12-16 hours at 4°C with agitation. Primary antibodies were diluted (1:1000) in fresh blocking buffer.

After incubation, blots were washed 5 times for 5 minutes each in TBST, incubated with secondary antibody in blocking buffer for 1 hour with agitation, and finally washed with TBST an additional 6 times for 5 minutes each. Chemiluminescent signals were developed with SuperSignal™ West Pico PLUS substrate for 5 minutes before imaging. One additional blot was developed with SuperSignal™ West Femto maximum sensitivity substrate (Thermo, 34094) to probe for potentially weak signals. The following primary antibodies were used: rabbit anti-AGO2 (Abcam, ab186733), rabbit anti-CD9 (Abcam, ab236630), rabbit anti-CD63 (Abcam, ab134045), rabbit anti-FLOT1 (Abcam, ab133497), rabbit anti-HSP90AB1 (Abcam, ab32568), rabbit anti-CANX (Cell Signaling Technology, 2679), and rabbit anti-TF (Cell Signaling Technology, 35293). The following secondary antibody was used: goat anti-rabbit IgG, HRP-conjugated (1:20000, Thermo, 31460).

Total protein staining. After separating proteins with SDS-PAGE, TFF gels were silver-stained with the Pierce™ Silver Stain Kit (Thermo, 24612), and UC gels fluorescently stained using the Revert™ 700 total protein staining kit (Licor, 926-11010), following the manufacturer's instructions. Gels were imaged on a Bio-Rad Chemidoc system using the silver stain program for silver-stained gels, or StarBright™ B700 program for fluorescently stained gels. Silver-stained gels were uniformly processed in ImageJ 1.54g (Java 1.8.0_345) using a combination of brightness/contrast adjustment, bandpass filtering, and the "enhance contrast" function to reduce overstaining and improve band clarity. Image adjustments did not alter relative protein abundance or band presence/absence.

Conventional negative stain transmission electron microscopy (TEM). EP samples were fixed in 2% (v/v) paraformaldehyde (Electron Microscopy Sciences, 15710) for 20 minutes at room temperature then adsorbed onto 200 mesh formvar coated gold grids (Electron Microscopy Sciences, FCF200-AU) by flotation of the grids on 20 μL droplets of fixed sample for 15 minutes. Grids were washed on three 20 μL droplets of TEM-grade PBS followed by two 20 μL droplets of

View Article Online
DOI: 10.1039/D6NR01765G

HPLC grade water, blotting with filter paper after each wash. Grids were stained with contrast agent (1% uranyl acetate (Fluka, 94260)) for 5 minutes, air-dried, then imaged on a JEOL JEM-1400Flash at 100 kV.

Immunogold TEM. EP samples were fixed and adsorbed onto formvar coated gold grids as described above. For blocking, grids were transferred to 20 μL droplets of 1% BSA (w/v) (Aurion, 900.011) diluted in PBS then incubated at RT for 30 minutes. Without washing, grids were transferred to 20 μL droplets of either primary antibody (1:100 Abcam, ab186733 or ab133497) diluted in 1% BSA, or 1% BSA only (negative control), then incubated overnight at 4°C in a Petri dish containing a moist wipe. After primary antibody incubation, grids were washed with three 20 μL droplets of 0.1% BSA, blotted in-between each wash, then transferred to 20 μL droplets of diluted 10 nm gold-conjugated goat anti-rabbit secondary antibody (1:20 Aurion, 25109) and incubated at room temperature for 1 hour. Grids were washed with three 20 μL droplets of 0.1% BSA in PBS, three 20 μL droplets of HPLC grade water, then stained for contrast with 1% uranyl acetate for 5 minutes.

SNA-I lectin-gold TEM. Exomere samples were fixed, adsorbed, and blocked as before. Instead of primary antibody incubation, samples were incubated with 5 nm gold-conjugated SNA-I lectin, diluted 1:4 (v/v) in 1% BSA in PBS (Ey Labs, GP-6802-5), for 30 minutes at RT. Grids were washed with three 20 μL droplets of PBS followed by three 20 μL droplets of HPLC-grade water, then stained for contrast with 1% uranyl acetate. A 1 mg/mL BSA-only grid was prepared as a negative control. Highly sialylated bovine fetuin protein (Millipore Sigma, F2379) was prepared as a positive control. On a fourth grid, exomeres were first incubated with 1 mg/mL unlabeled SNA-I (Ey-labs, L-6802-2) in PBS at RT for 30 minutes, followed by incubation with gold-conjugated SNA-I. This grid served as a control for SNA-I binding specificity.

Particle size estimation. UC and TFF exomere particle diameters were estimated using the ImageJ 1.54g (Java 1.8.0_345) “analyze > measure” tool on particles from 3 separate TEM micrographs each. All particles were measured north to south to reduce bias. The measurement

View Article Online
DOI: 10.1039/D6NR01765G

scales were set using the pixel width of the scale bars on the original TEM JPG files. All measurements from each set of micrographs were pooled prior to analysis.

RNA protection assay. For RNase A only treatment, EP samples were treated with 1 μg/mL RNase A (Thermo, EN0531), briefly vortexed, then incubated at 37°C for 30 minutes. For Proteinase K/RNase A treatment, samples were treated with 1 μg/mL Proteinase K (Qiagen, RP103B), briefly vortexed, then heated at 56°C for 10 minutes. Samples were immediately quenched with 1X EDTA-free protease inhibitor cocktail (Thermo, 78425) for 5 minutes at RT to inactivate Proteinase K, then treated with 1 μg/mL RNase A as before. For Triton X-100/RNase A treatment, Triton X-100 was added to samples at a final ratio of 0.075% (v/v), vortexed for 30 seconds, then immediately treated with 1 μg/mL RNase A. Optimal Triton X-100 conditions to disrupt EV membranes were determined elsewhere.[28] As a control for cotreatment effects, GAPDH siRNA from the Qubit™ microRNA assay kit (Thermo, Q32880) was evaluated in parallel. Reagents were prepared fresh each day. A concentration of 1 μg/mL each of RNase A and Proteinase K was selected with consideration of the minimum effective concentration needed to completely degrade the GAPDH siRNA control in 30 minutes, and the approximate physiological levels of serine proteases and ribonucleases found in human serum.[29,30]

Small RNA extraction and sizing. Small RNAs were isolated from TFF EP samples using the miRNeasy micro kit (Qiagen, 217084) standard protocol, with minor modifications. 120-360 μL of particle suspension was used as input instead of EP pellets. Purified small RNAs were eluted in 30 μL of nuclease-free water after allowing the silica columns to soak for 2 minutes. This modification improved elution volume consistency across samples. RNA size distributions were qualitatively assessed using the Agilent 5200 Fragment Analyzer and small RNA kit (Agilent, DNF-470-0275). Briefly, purified RNA samples were diluted in nuclease-free water to obtain concentrations within the dynamic range of the assay (25-2500 pg/μL for microRNA region). Samples and reference ladder were heat-denatured in a thermal cycler at 70°C for 10 minutes then immediately cooled to 4°C and held until use. 2 μL of each sample or ladder was added to 18 μL of diluent marker,

View Article Online
DOI: 10.1039/D6NR01765G

thoroughly mixed, then separated at 8.0 kV for 24 minutes using protocol DNF-470-33 for a 33 cm capillary array.

Proteinase K activity assay. 2 μg of BSA dissolved in 25 mM PBS-H was treated with either 1 μg/mL Proteinase K or Proteinase K and 1X protease inhibitor, briefly vortexed, then incubated at 56°C for 10 minutes. One untreated sample was processed in parallel as a control. Proteins were denatured and separated using SDS-PAGE as previously described. The gel was stained with QC colloidal Coomassie stain (Bio-Rad, 1610803) and visualized on a Bio-Rad Chemidoc system using the Coomassie Blue program.

RNase A activity assay. 300 ng of GAPDH siRNA and a custom oligonucleotide (Eurofins Genomics, sequence: 5' AUAUAGACAUUACUUAGUAAA 3') were separately diluted in 25 mM PBS-H. Each sample was treated with 1 μg/mL RNase A, briefly vortexed, then incubated at 37°C for 30 minutes. One untreated sample of each RNA was used as a control. After incubation, RNA was extracted using the miRNeasy micro kit as described above. RNA was separated using denaturing nucleic acid PAGE on a 10% TBE-Urea precast gel (Bio-Rad, 4566033) then visualized with SYBR™ Gold (1:10000, Thermo, S11494). The stained gel was imaged on a Bio-Rad Chemidoc system using the SYBR™ Gold program.

RNA library generation and sequencing. Small RNAs isolated from TFF EPs were cleared of residual contaminants (Zymo Research, R1013) then used as input for library prep. All RNA sequencing was performed at the Michigan State University Research Technology Support Facility Genomics Core. Libraries were prepared using the Lexogen small RNA-seq library preparation kit for Illumina (Lexogen, 052), following manufacturer's instructions. Completed libraries were quality controlled and quantified using a combination of Biotium AccuGreen™ high sensitivity dsDNA (Biotium, 31066) and Agilent 4200 Tapestation HS DNA1000 (Agilent, 5067) assays. Libraries were normalized by concentration and pooled in equimolar amounts. The pooled library was then cleaned to remove small fragments and adapter dimers using the Lexogen Purification Module protocol (Lexogen, 022.24) with magnetic beads at a 1.3:1 (v/v) bead-to-library ratio. The library pool was sequenced using an Element Biosciences AVITI Cloudbreak Freestyle 150 cycle medium

View Article Online
DOI: 10.1039/D6NR01765G

output kit (Element Biosciences, 860-00014). Sequencing was performed in a 1x50 bp single read format. Base calling was done by AVITI OS v3.3.2 followed by demultiplexing and conversion to FastQ format using Element Biosciences bases2fastq v2.1.0.

Small RNA sequencing analysis. Analyses were performed by the Michigan State University Bioinformatics Core. 3' adapters were removed from all reads using cutadapt.[31] Untrimmed reads and reads with a length less than 15 bp after trimming were discarded. Reads from each sample were mapped to known miRNAs of the human genome using miRBase to obtain read counts for each miRNA.[32] This step was carried out using the miRDeep2 pipeline.[33] The DESeq2 package in R was used to find differentially expressed miRNAs with exomeres taken as the baseline group for $\log_2$ fold change (LFC), i.e., $\log_2$(F2 EV mean count/F4 exomere mean count).[34] The lfcShrink() function was called to shrink the effect size of LFC. The Wald test was used to calculate p-values. Adjusted p-values were calculated using the Benjamini-Hochberg (BH) procedure for FDR control. Differentially expressed miRNAs were taken to be those with an adjusted p-value < 0.05. The counts were normalized using the median of ratios method to account for variations in library size/sequencing depth as well as sample composition.

Reverse transcription quantitative real-time PCR (RT-qPCR). RNA extracted from TFF EP samples using the miRNeasy micro kit (Qiagen, 217084) was cleared of contaminants (Zymo Research, R1013) then used as input. The following TaqMan™ advanced miRNA assays (Thermo, A25576) were used: 478735_mir (hsa-miR-1908-5p), 483118_mir (hsa-miR-12136), 477992_mir (hsa-miR-24-3p), and 477982_mir (hsa-miR-222-3p). Briefly, RNA was 3' polyadenylated and 5' adapter ligated then reverse transcribed to generate cDNA using the TaqMan™ Advanced miRNA cDNA synthesis kit (Thermo, A28007). After cDNA amplification using the miR-Amp reaction, qPCR was run on a CFX96 (Bio-Rad). Data were analyzed using the $\Delta\Delta C_t$ method with normalization to the geometric mean of the C_t values for hsa-miR-24-3p and hsa-miR-222-3p in each sample. F2 EVs were taken as the basis.

View Article Online
DOI: 10.1039/D6NR01765G

Statistics. To determine significant differences in TFF fraction total protein abundance, a Kruskal-Wallis nonparametric test with Dunn's multiple comparisons at α=0.05 was run using R 4.2.2 in BioRender. Sample group means (n=8 per group) for F2, F3, and F4 were compared to F1.

Results

Recognizing the potential applications of exomeres, we wanted to determine if TFF, which is more compatible with industrial scale bioprocesses than UC and AF4, could reproducibly isolate exomeres from conditioned media. Using the typical size ranges of EVs and exomeres as a guide, we developed a bench-scale tandem TFF process to separate exomeres from other EPs (**Fig. 1**). We then performed biophysical and molecular characterization on particles isolated from multiple steps in the purification process and benchmarked them against EPs obtained using differential UC.

Particle retention modeling informs TFF membrane selection

The selection of TFF membranes was informed by particle retention models that assumed a log-normal distribution of pores. Log-normal probability correlations effectively predict the sieving behaviors of synthetic ultrafiltration membranes.[35] For a 35 nm particle, assumed to be spherical and isotropic, rejection coefficients of 90%, 49%, and 28% were calculated for 5, 15, and 25 nm mean pore size filters, respectively (**Supp. Fig. 2**). We subsequently hypothesized that exomeres could be selectively enriched between a 5 nm and 15 nm filter (designated as retentate fraction F4 - 100 kDa MWCO). For the 15 nm membrane (300 kDa - F3), the calculated rejection coefficients for small (~60 nm) and large (~100 nm) EVs were 72% and 88%, respectively. This membrane was used immediately prior to the terminal filter. Three additional filters sized at 185, 50, and 25 nm (0.2 μm, 0.05 μm - F1, 500 kDa - F2), were used to clarify the conditioned media and isolate EVs upstream of exomeres.

View Article Online
DOI: 10.1039/D6NR01765G

TFF exomeres are highly pure and enriched in RNAi proteins

Exomere enrichment in fraction F4 was first confirmed using Western blot. F4 was negative for EV markers associated with endocytosis and vesicle trafficking (CD9, CD63, FLOT1) but enriched in RNAi-associated proteins (AGO2, HSP90AB1) (**Fig. 2A**). HSP90 has been proposed as a potential biomarker for mammalian exomeres.[9] In the cell, HSP90 helps load small RNA duplexes onto AGO2 in an ATP-dependent manner and also aids in its targeting to processing bodies and stress granules.[36,37] F3, containing a less concentrated population of non-membranous nanoparticles, showed faint signals for AGO2 and HSP90 and lacked EV markers. Comparable trends in the depletion and enrichment of protein markers were observed in small EV (sEV) and exomere (EXOM) fractions isolated by UC (**Fig. 2B**). F4 had significantly higher protein content than other fractions, especially compared to large EVs in F1, suggesting that F4 contained protein-rich, non-vesicular particles (**Fig. 2C**).

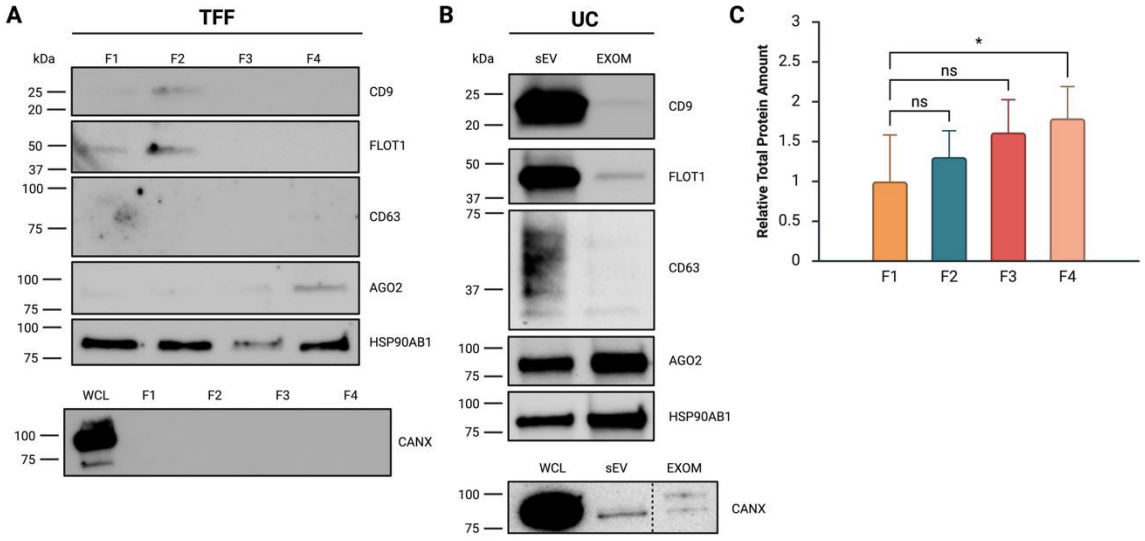

Figure 2: TFF F4 exomeres are comparable in purity and molecular content to UC exomeres. A. Western blots of TFF EV (F1, F2) and NVEP fractions (F3, F4). Representative blot of three biological replicates shown. **B.** Western blots of differential UC small EVs (sEV) and exomeres (EXOM). Representative blot of two biological replicates shown. The endoplasmic reticulum marker Calnexin (CANX) was tested once in each case as a negative control for co-purification of cell debris. Blots were cropped and uniformly processed in ImageJ 1.54g (Java 1.8.0_345). Unprocessed blots can be found in **Supp. Fig. 3**. **C.** Relative total protein content of F1-F4. Data are presented as mean ± SEM and represent eight biological replicates. A Kruskal-Wallis nonparametric test with Dunn's multiple comparisons at α=0.05 was run to determine significant differences, * P < 0.05. Figure created with BioRender.com.

View Article Online
DOI: 10.1039/D6NR01765G

Total protein staining revealed comparable enrichment of proteins near 15 kDa and 100-150 kDa in both TFF and UC exomere fractions (**Supp. Fig. 3**). Previously, E-PHA lectin blotting detected a high molecular weight glycoprotein near 150 kDa in AsPC-1 and MDA-MB-4175 exomeres.[9] TFF appeared to yield purer exomeres than UC, as CD9, FLOT1, and CANX (EV and cell debris markers) were consistently detectable at low levels in the UC fractions. We probed TFF fractions F2-F4 on an additional blot with a maximum sensitivity, low-femtogram ECL substrate to confirm that the lack of EV proteins was a function of isolate purity and not inadequate protein loading. We found F3 and F4 to be absent of EV markers in this experiment as well (**Supp. Fig. 3**).

Recognizing that soluble and aggregated proteins had the potential to copurify with exomeres, especially those in high abundance such as the media supplement transferrin, we probed for transferrin using Western blot then calculated the average mass of copurifying transferrin by taking the known amount added to the unconditioned media as a basis and performing band densitometry. On average, ~24% and ~38% of the total protein mass for TFF and UC exomere isolates was transferrin, respectively. While these data reveal that TFF isolation does not remove all contaminants from the exomere fraction, they further support our claim that TFF yields purer exomeres than those isolated by UC (**Supp. Fig. 3**). Finally, to assess exomere yield, we constructed a normalized metric to use as a proxy for particle count, transferrin-adjusted total protein per mL of conditioned media, and found that TFF tended to isolate more total protein than UC (**Supp. Fig. 3**).

AGO2 and α2,6-linked sialic acid localize to crenated structures within the TFF exomere fraction

TEM of EVs and exomeres revealed distinct particle morphologies. Both UC and TFF EVs exhibited the typical cup-like structure.[6] TFF appeared to yield more structurally intact EVs with less aggregation. TFF and UC exomere fractions contained particles of comparable size and morphology. Particle sizes from the UC exomere fraction (49.8 ± 22.0 nm, SD) and TFF exomere fraction (45.6 ± 10.7 nm, SD) were determined by manual measurement of particle diameters from several TEM micrographs (**Supp. Fig. 4**). We attempted to measure particle size using a Particle

View Article Online
DOI: 10.1039/D6NR01765G

Metrix ZetaView® nanoparticle tracking analyzer (NTA) but could not detect particles smaller than 50 nm in either UC or TFF exomere fractions, likely due to limitations regarding the detection of very small particles with low refractive indices. TFF produced exomeres with less apparent contamination, as evidenced by the absence of small amorphous aggregates frequently observed in the UC micrographs (**Fig. 3A** and **3B**).

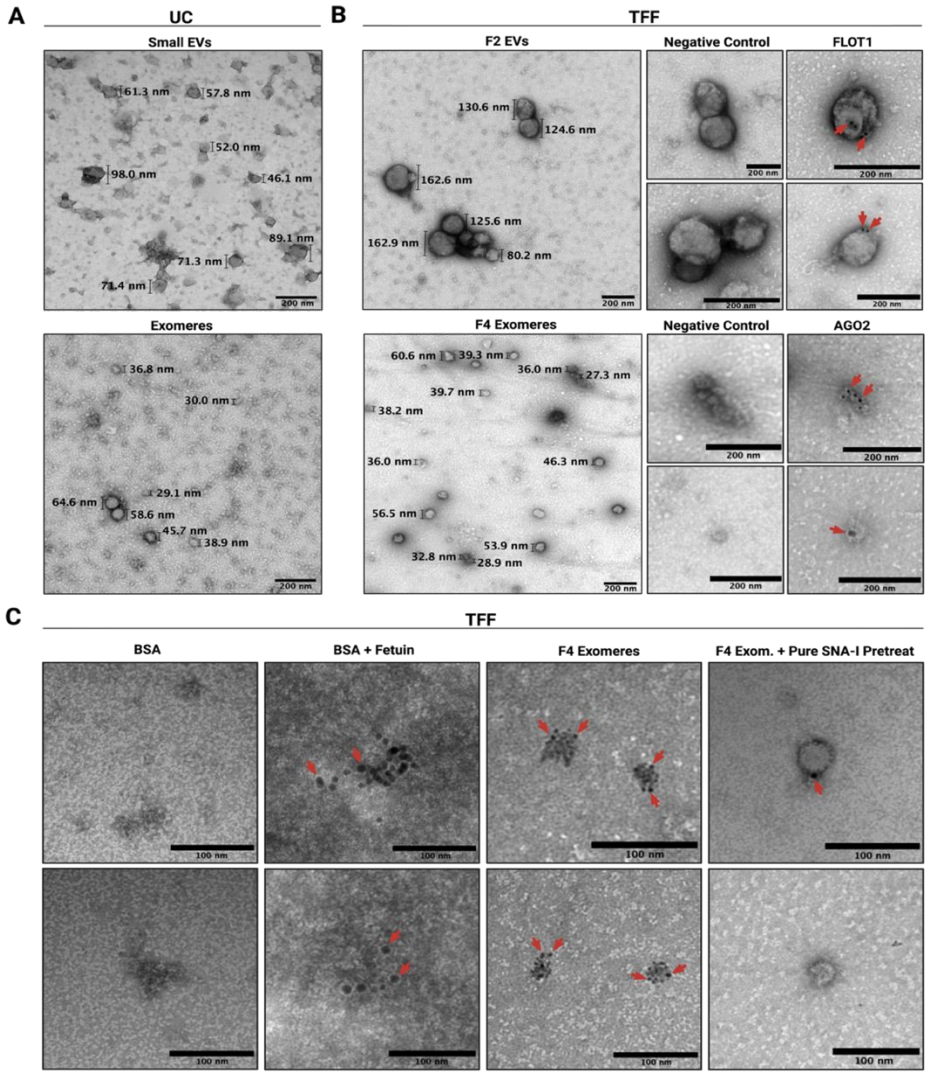

Figure 3: TFF isolates exomeres morphologically similar to those isolated by UC. A. Negative-stain TEM of UC sEV and exomere fractions. **B.** Immunogold TEM of TFF EV (F2) and exomere (F4) fractions. **C.** SNA-I lectin gold staining of TFF exomeres. BSA, BSA and fetuin, and pure SNA-I pretreatment were used as controls. Immunogold and lectin-gold experiments were performed twice on independent TFF fractions. Uncropped micrographs are provided in **Supp. Fig. 4,5**. Figure created with BioRender.com.

View Article Online
DOI: 10.1039/D6NR01765G

Immunogold staining with FLOT1 confirmed the presence of EVs in TFF F2 (**Fig. 3B**). Treatment of F4 with gold-conjugated AGO2 resulted in the staining of 35-40 nm particles with punctate centers and crenated edges. These structures occurred individually and as aggregates (**Fig. 3B**). Similar structures were observed in our UC fraction as well as in prior work on DiFi exomeres.[6,14] To further investigate if particles stained by AGO2 were exomeres, we performed lectin-gold staining with gold-conjugated SNA-I targeting terminally linked α2,6 sialic acid. Exomeres are major carriers of sialylated glycoproteins.[9] Lectin-gold particles localized to the same types of punctate structures as in the AGO2 staining. We confirmed the specificity of SNA-I for α2,6-linked sialic acid using sia-free BSA and a highly-sialylated bovine serum protein, fetuin (**Fig. 3C**). As expected, SNA-I bound to aggregates of fetuin but showed no binding in the BSA-only control. Pretreatment with unlabeled SNA-I virtually abolished gold labeling of exomeres, indicating that sialic acid sites were already occupied by unconjugated lectin and therefore inaccessible to the conjugate (**Fig. 3C**). The sialoglycoprotein Galectin-3-binding protein (LGALS3BP) is enriched in exomeres and natively self-assembles into ring-like decamers 30-40 nm in size.[9,38] The structures identified in our lectin-gold experiment were of similar size and strongly bound SNA-I at their perimeters. This suggests that heavily glycosylated proteins might support cell surface-exomere interactions.[9] These crenated structures were also present in F2 at moderate abundance, indicating that exomeres can copurify with EVs (**Supp. Fig. 4**), as would be expected.

To further investigate the contents of our TFF fractions, we separated F2 EVs and F4 exomeres with an IZON 20 nm gravity-flow SEC column then performed protein and particle structure measurements on the various fractions. In alignment with our prior analyses of the bulk TFF samples, SEC fractions 2-9 of F2 EVs, but not F4 exomeres, were enriched in vesicle and membrane marker CD9 as detected by native dot blot. We found a sharp protein peak in fraction 9 of F2 EVs, which was absent in the exomere fraction, and verified that this fraction was vesicle-rich using TEM (**Supp. Fig. 6, 7**). Building on the hypothesis that LGALS3BP oligomers may be structurally important to exomeres, we performed native dot blots on F4 exomere SEC fractions using an LGALS3BP polyclonal antibody and found this protein to be natively accessible in fractions

View Article Online
DOI: 10.1039/D6NR01765G

2-17, with the majority eluting in fractions 2-6. TEM of fractions 3, 9, 12, and 21 revealed various sizes of crenated particles that had a similar overall structure to those found to be strongly stained with SNA-I lectin and weakly stained by AGO2 in our gold-conjugate experiments (**Supp Fig. 7**). To identify the TFF F4 fractions containing AGO2, we performed a denaturing dot blot on the F4 exomere SEC fractions and detected AGO2 in fractions 17 and 18. Surprisingly, we did not detect AGO2 in the earlier fractions found to be highly enriched in LGALS3BP.

TFF exomeres protect their endogenous RNAs from nuclease degradation

We next profiled the small RNA content of TFF EVs and exomeres. RNAs in the size range of miRNAs were abundant in both fractions. In contrast, larger RNAs (80-200 nt) were more prevalent in EVs. We investigated the accessibility of the RNAs using an RNase protection assay, in which fractions were treated with combinations of RNase A, Proteinase K, and Triton X-100. Exomere RNAs were remarkably resistant to enzymatic degradation, even in the presence of surfactant or protease. As expected, EV RNAs were substantially degraded upon treatment with Triton X-100, a known EV membrane disruptor (**Fig. 4A, 4B**).[28] These data reinforce that exomeres lack membranes but also reveal that exomeres package small RNAs in a highly stable, nuclease-resistant complex. Using a control 21-mer GAPDH siRNA, we confirmed that RNase A was still active in the presence of Triton X-100 and Proteinase K (**Fig. 4C)**, reinforcing our contention that exomeres protect their contained miRNAs from RNase degradation through steric or other mechanisms.

View Article Online
DOI: 10.1039/D6NR01765G

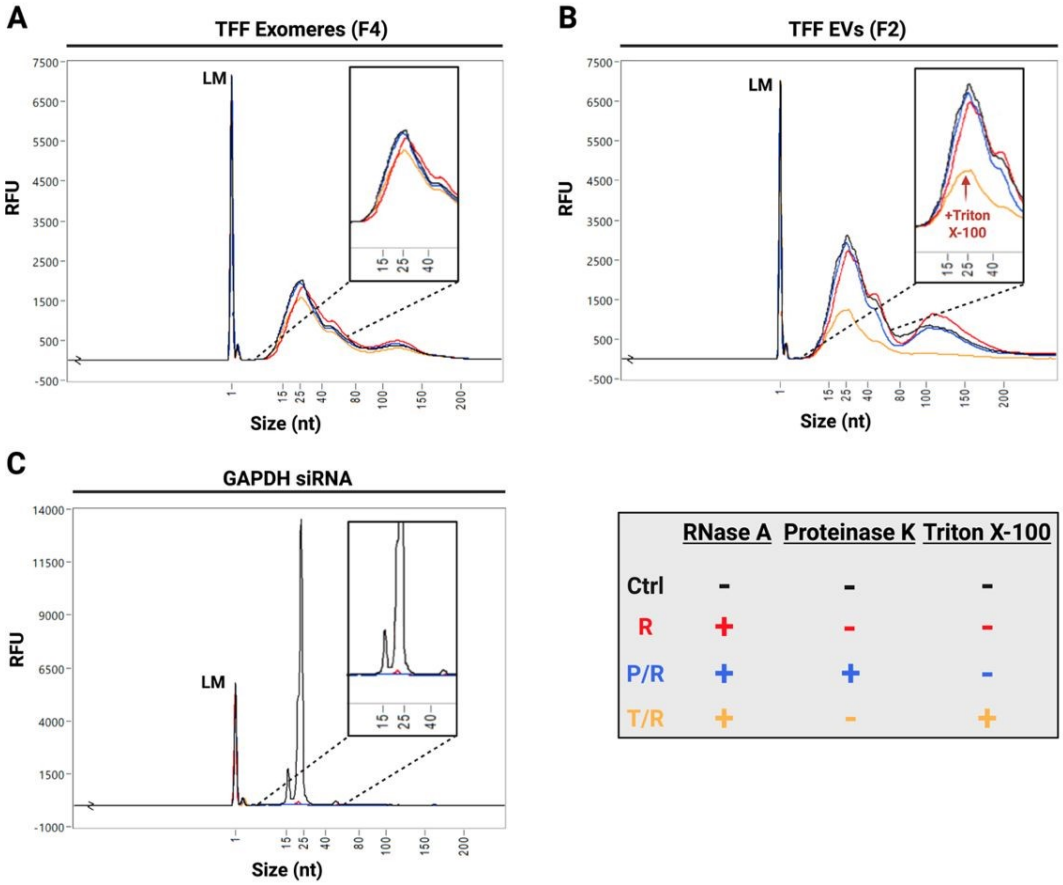

Figure 4: TFF exomere RNAs are protected against enzymatic degradation in the presence of protease and surfactant. Representative fragment analyzer traces of small RNAs isolated from **A.** TFF exomeres (F4) and **B.** TFF EVs (F2). Treatment conditions: Ctrl (Control), R (RNase A only), P/R (Proteinase K/RNase A), T/R (Triton X-100/RNase A). **C.** GAPDH siRNA measured in parallel as a control. Replicate experiments can be found in **Supp. Fig. 8**. Figure created with BioRender.com.

Proteinase K activity was verified by treating BSA with either Proteinase K, or Proteinase K and protease inhibitor, followed by SDS-PAGE and Coomassie blue staining. As expected, Proteinase K degraded BSA, with degradation being limited by the presence of protease inhibitor (**Supp. Fig. 8**). We also confirmed that RNase A could cleave single- and double-stranded RNAs in our TFF buffer (25 mM PBS-H), using GAPDH siRNA for the double-strand and a scrambled RNA oligomer designed to avoid hairpin formation and palindromic basepairing for the single-strand. RNase A degraded both RNAs but showed a stronger activity against the single-stranded

View Article Online
DOI: 10.1039/D6NR01765G

RNA, further indicating that exomere RNAs, which are likely single-stranded, are protected by a nuclease-resistant complex (**Supp. Fig. 8**).

TFF EVs and exomeres are enriched in distinct populations of miRNAs

To confirm the presence of miRNAs in our TFF EV and exomere samples, we performed RNA sequencing on the F2 and F4 small RNA fractions. Overall, sequencing reads for EVs and exomeres were successfully mapped to 812 mature miRNAs using the miRBase microRNA database.[32] 27 miRNAs were differentially expressed, six of which were significantly more enriched in exomeres (**Fig. 5A**). miR-4516 and miR-3960 were the most abundant miRNAs in each fraction, accounting for 77.5% and 84.5% of the total read count across replicates for EVs and exomeres, respectively. miR-320a-3p, a highly abundant miRNA in DiFi exomeres and supermeres[7], was also abundant in our TFF exomeres as well as differentially expressed compared to TFF EVs (**Fig. 5A** and **5B**). Interestingly, miR-30a-3p was found exclusively in the exomere fraction and might therefore serve as an exomere-specific biomarker.

As we and others continue to explore the function and utility of EPs, it will become even more critical to establish how best to quantify the molecular components of isolated particles. To that end, we sought to determine if any miRNAs in our isolated EPs could serve as reference miRNAs, showing reasonably constant and high abundance and allowing for standardization of the levels of other miRNAs across different EP types. Selection criteria for targets to validate were: fold change, FDR adjusted p-value, and a normalized mean read count of at least 100 reads for each sample group, suggested as a suitable threshold for selecting miRNA candidates for qPCR validation.[39] From the literature and our RNA-seq data, miR-222-3p and miR-24-3p, abundant and stably expressed miRNAs found in DiFi cells, sEVs, exomeres, and supermeres[7], were identified as potential candidates. miR-222-3p ranked among the top 30 most abundant miRNAs in both TFF EVs and exomeres and showed comparable abundance between samples based on normalized read counts and fold change (**Fig. 5C**). This observation was further confirmed using TaqMan™ probe RT-qPCR, indicating that both miR-222-3p and miR-24-3p may be appropriate reference molecules for quantifying miRNA abundance across different EP types moving forward. We verified

View Article Online
DOI: 10.1039/D6NR01765G

that differential abundance trends were consistent between RNA-seq and RT-qPCR using miR-1908-5p and miR-12136 normalized to the average expression (geometric mean) of miR-222-3p and miR-24-3p (**Supp. Fig. 9**). Overall, our findings reveal that exomeres isolated by tandem TFF are biologically comparable to exomeres isolated by UC (by us and others), of greater purity than those isolated by UC, and contain small RNAs that are resistant to RNase degradation even in the presence of surfactant and protease.

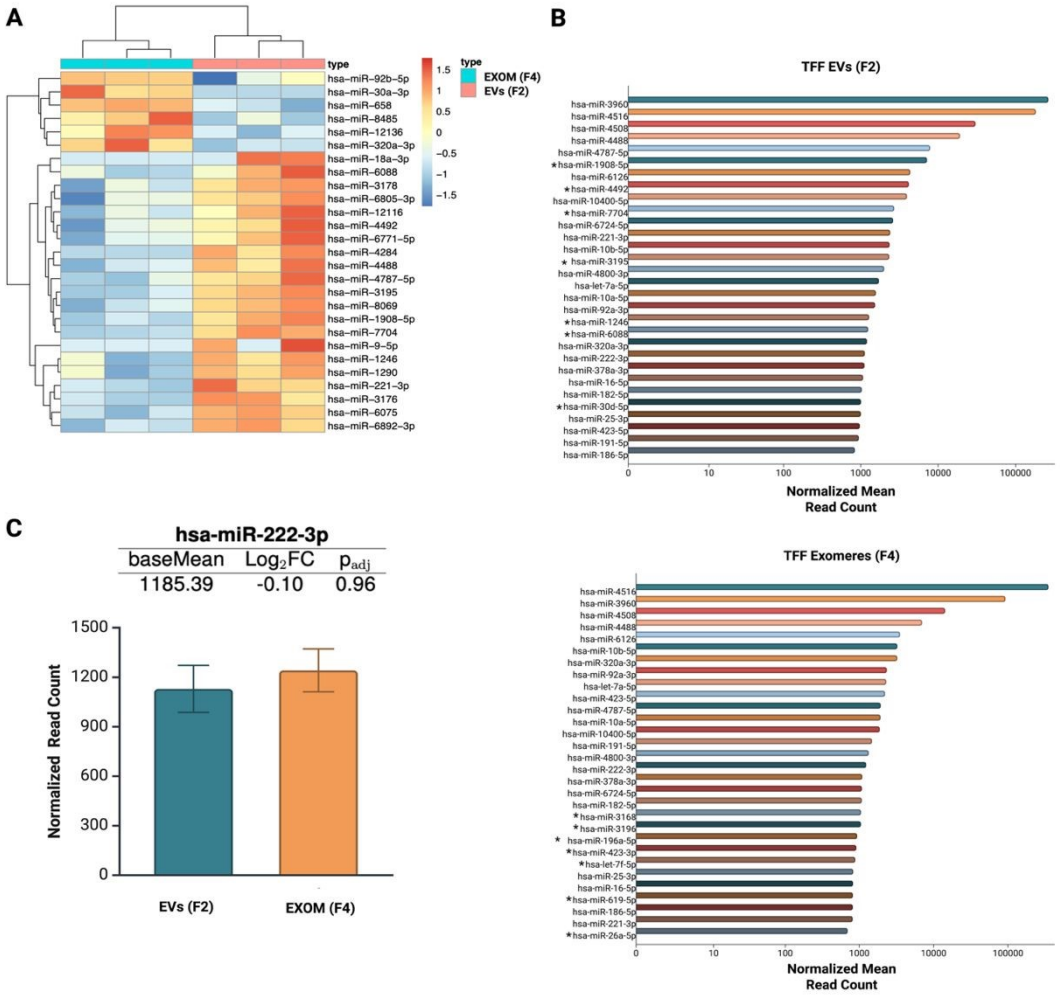

Figure 5: TFF EVs and exomeres are enriched in distinct populations of miRNAs. A. Differentially expressed miRNAs between EVs and exomeres, $p_{adj} < 0.05$. Data represent three biological replicates. **B.** 30 most abundant miRNAs in EVs (top) and exomeres (bottom) based on normalized mean read counts. Asterisks (*) indicate miRNAs unique to EVs (top) or exomeres (bottom) within the 30 most abundant. **C.** Differential expression of hsa-miR-222-3p. Data are presented as mean ± SD and represent three biological replicates. Data were normalized using the median of ratios method. Figure created with BioRender.com.

View Article Online
DOI: 10.1039/D6NR01765G

Discussion

Ultracentrifugation is currently the most well-described approach for isolating exomeres from conditioned media and is more accessible than AF4. However, UC is time-intensive, risks exomere co-sedimentation with EVs and other components, and cannot easily be scaled to produce pilot or production scale quantities of exomeres. Recently, FPLC-SEC was introduced as a more scalable alternative to UC and AF4 for the isolation of exomeres and supermeres, underscoring the importance of studying NVEPs and the need for improved isolation methods.[14] In this study, we developed a tandem TFF process to i) provide another rapid isolation method for mammalian exomeres, and ii) assess the feasibility of industrially compatible filtration processes for isolating NVEPs. Highly pure exomeres were successfully isolated within hours of media harvest, with 360 mL of conditioned media routinely processed in as little as three hours. Indeed, other efforts to apply TFF to isolate NVEPs are emerging[40], reinforcing the potential of our purification approach.

TFF exomeres displayed molecular and morphological features consistent with exomeres isolated by UC, including the enrichment of RNAi proteins AGO2 and HSP90AB1 and the glycoprotein LGALS3BP. The absence of FLOT1, CD9, and CANX signals on Western blots, as well as reduced TEM background, suggested that TFF produced fractions of higher purity compared to UC. Contaminating proteins such as transferrin copurified with UC exomeres at higher concentrations than those isolated using TFF, further demonstrating that TFF improved exomere purity. TFF also appeared to yield exomeres of more uniform particle size (as measured on TEM micrographs), which can be attributed to the removal of aggregated particles by the upstream tandem filters and free protein contaminants in the exomere retentate by diafiltration.

SNA-I lectin-gold staining targeting α2,6-linked sialic acid resulted in the localization of gold particles to the exomere perimeter, suggesting a non-random distribution of sialic acid on the particle surface that may serve to mediate interactions with recipient cells. Indeed, when attempting to confirm the presence of LGALS3BP in TFF exomeres, we found it to be highly accessible using native dot blot, suggesting that these sialylated glycans would also be available to interact with the surface of cells. LGALS3BP self-assembles into 30-40 nm ring-like oligomers, possibly enabling

View Article Online
DOI: 10.1039/D6NR01765G

the encapsulation of protein complexes.[38] While the staining efficiency was relatively low, the localization of gold-conjugated AGO2 to the same types of crenated structures stained by SNA-I makes it tempting to speculate that glycoprotein-AGO2 complexes could be a fundamental constituent of the exomere. These observations may further suggest that the indented core of the exomere is a biological feature rather than an experimental artifact.

We performed gravity-flow SEC on our TFF isolates to further investigate their contents and were intrigued to find that exomeres consist of a distribution of small non-vesicular particles with the same general morphology (as measured by TEM). Interestingly, AGO2 (as detected by dot blot) was present only in SEC fractions 17 and 18 and not those most enriched in LGALS3BP. This is not entirely unexpected considering that i) the immunogold staining efficiency was low, suggesting that AGO2 in the LGALS3BP-rich fractions could be below the limit of detection, and ii) exomeres were exceptionally difficult to degrade in our later RNA protection experiments, implying that mild denaturing conditions may not have been sufficient to render the AGO2 epitope accessible. Nevertheless, we find that exomeres appear to consist of a distribution of differently sized NVEPs, and this may allow cargo molecules to partition into subsets of these particles based on their relative size. Indeed, LGALS3BP dimers can assemble into particles of different sizes, which would afford this flexibility.[38] Until individual particles within NVEP fractions are better characterized, attribution of function to the bulk samples should be approached with caution. A recent report found that 81% of the exomere protein mass can be attributed to histone and 20S proteasome complexes, and supermeres are largely absent of macromolecular complexes[41], suggesting that NVEPs may be more heterogeneous than initially thought. We expect SEC and similar high-resolution purification approaches to be critical in future studies for separating and characterizing these different NVEP subgroups.

Exomeres naturally transport components of RNAi, making them promising candidates for RNAi therapeutics and biomarker discovery (e.g., of differentially incorporated miRNAs). Because miRNAs must persist in circulation to be functional in target tissues, we attempted to degrade the small RNAs in TFF EVs and exomeres using RNase A combined with either the membrane

View Article Online
DOI: 10.1039/D6NR01765G

disruptor Triton X-100 or the broad-spectrum protease, Proteinase K. Remarkably, exomere RNAs persisted through each treatment. Conversely, EV RNAs were substantially degraded by RNase A after Triton X-100 treatment, reinforcing that exomeres and EVs differ in their structure and packaging of contained RNAs and therefore may also differ in their endocytosis and processing by recipient cells.

It is unclear if the protection from RNase A observed in our experiments is generalizable to all miRNAs. RNase A is a distributive enzyme with three nucleotide binding subsites (B1-B3) that coordinate to cleave the 3' phosphodiester bond of the pyrimidine bound by B1.[42] B1 binds only pyrimidines, whereas B2 and B3 bind all bases, with preferences for adenine (B2) and purines (B3), respectively.[42,43] miRNA susceptibility to RNase A is therefore dependent on its pyrimidine content and, to a lesser extent, the identity of the adjacent bases bound by B2 and B3. The most abundant exomere miRNA in this study, miR-4516, contains only one potential cleavage site (base 12 from the 5' end). The second most abundant miRNA, miR-3960, contains four sites (bases 3, 6, 9, and 15 from the 5' end). Neither miR-4516 nor miR-3960 have adenines in the preferred locations for B2. Because these two miRNAs comprise over 80% of the total exomere miRNA reads, it is plausible that sequence effects that preclude RNase A binding, in addition to the stability provided by the exomere itself, contributed to the remarkable amount of RNA protection observed here. This might further suggest that exomeres package miRNAs with inherent resistance to endonucleases to maximize the likelihood of sending a successful signal between the exomere producing cells and their recipients. Interestingly, miR-4516 promotes glioblastoma progression by targeting a tumor suppressor of the Hippo pathway, *PTPN14*, suggesting that exomere miR-4516 might be of diagnostic value in brain cancer.[44] Future studies using a panel of RNases with different sequence specificity will help to determine whether exomeres protect certain miRNAs more than others.

RNA sequencing confirmed that miRNAs were abundant in both particle types. A total of 812 mature miRNAs were successfully mapped across EV and exomere sequence reads, six of which were preferentially associated with exomeres. Surprisingly, miR-30a-3p was found only in the exomere fractions across all replicates. miR-30a-3p has been shown to suppress the invasion

View Article Online
DOI: 10.1039/D6NR01765G

potential of bladder cancer cells and improve their chemosensitivity *in vitro*, suggesting a potential therapeutic role for exomeres in cancer treatment.[45] It is worth noting that the most abundant miRNAs in each fraction had exceptionally high GC content (>85%, top 4 miRNAs ranked by normalized mean read count). High GC content in the canonical miRNA seed region (i.e., positions 2-8 from the 5' end) and the extended seed region (positions 4-10) strongly correlates with perfect base pairing to the mRNA target, and an increase in the number of matched seed pairs improves the thermodynamic stability of the miRNA-mRNA duplex.[46] Given sufficient time for RISC to recruit deadenylation machinery, a translationally repressed transcript can further be destabilized and degraded, eliminating the possibility of its recovery via cytoplasmic polyadenylation.[47] For intercellular miRNAs that are i) in low adundance relative to intracellular levels and ii) susceptible to degradation by circulating nucleases, high GC content may be evolutionarily favored for enhancing potency and increasing the likelihood of complete target inactivation. This mechanism would be consistent with the known functions of EPs, as cells must communicate clear and active signals to neigboring cells to rapidly enact change in response to stress or other stimuli. To validate a subset of our sequencing results with RT-qPCR, we tested two differentially expressed miRNAs, miR-1908-5p and miR-12136, as well as two that were stably expressed, miR-24-3p and miR-222-3p, and found those results to be in general agreement with the RNA sequencing. As such, miR-24-3p and miR-222-3p appear to be useful endogenous controls for assays that require stable reference RNAs.

Our results further support that exomeres and EVs are produced through overlapping (due to shared molecular content) but distinct biogenesis mechanisms. Previous work demonstrated that sequence motifs direct some miRNAs to EVs, and their loading is mediated by a sumoylated form of the ribonucleoprotein hnRNPA2B1.[48] However, hnRNPA2B1 appears to preferentially associate with NVEPs.[7] AGO2 phosphorylation was previously found to regulate the packaging of certain miRNAs into exosomes.[49] We and others found AGO2 to be mainly associated with the non-vesicular fractions.[6–8] Further characterization of individual RNA-binding proteins in each EP fraction will be needed to better understand the biogenesis of different classes of EPs, as bulk

View Article Online
DOI: 10.1039/D6NR01765G

characterization obscures the link between specific intracellular signaling and sorting processes to the biogenesis of individual extracellular particles.

Moving forward, we are continuing to refine the TFF process for further purification and characterization of exomeres. Although exomeres must be collected in serum-free media, using ITS as a serum substitute complicated biophysical characterization because its protein components persisted through TFF. Transferrin has been shown to form fibrillar deposits on carbon-coated formvar surfaces in the size range of EVs, which may have complicated visual assessments of purity using TEM.[50] Additionally, we cannot completely rule out the presence of other extracellular particles in our exomere fraction. Lipoprotein complexes are secreted particles of similar size to exomeres. Intermediate-density lipoproteins (IDLs) and very-low-density lipoproteins (VLDLs) appear as 20-60 nm particles under TEM.[51] However, we are reasonably confident that the particles we isolated were exomeres, since i) HEK293 cells do not express apolipoproteins according to the Human Protein Atlas[52,53]; and ii) TEM grids containing only BSA, the blocking reagent for gold staining experiments, and fresh ITS media were free from particles with the exomere morphology.

We believe this separation process can be applied to other moderately viscous biofluids such as serum and lymph. miRNAs are well understood to be biomarkers for disease, with many being dysregulated in the serum of patients with cancer, cardiovascular disease, and nervous system disorders.[54] Lymph, which plays an important role in maintaining homeostasis and trafficking immune cells, carries a different distribution of miRNAs compared to other biofluids such as plasma.[55] TFF has already been employed to isolate protein complexes from plasma and Fraction IV, and EVs from lipoaspirate, suggesting that TFF could also be used to isolate exomeres and their miRNAs from these other biofluids.[19,56] The robust protection of miRNAs by exomeres suggests that exomeres have potential use as both circulating biomarkers and RNAi therapeutics.

Conclusions

This study describes a rapid and cost-effective bench-scale method to isolate highly pure EVs and exomeres from conditioned media, enabling further research toward applications in RNAi therapeutics. This study also demonstrates, for the first time, that exomeres protect their constituent

View Article Online
DOI: 10.1039/D6NR01765G

miRNAs more comprehensively from nuclease degradation than EVs, reinforcing that they likely play a complementary role to EVs in supporting intercellular communication.

Author contributions

TS contributed to conceptualization, formal analysis, investigation, methodology, writing the original draft, and reviewing/editing of the final work.

YH contributed to conceptualization, funding acquisition, investigation, methodology, and reviewing/editing of the final work.

OB contributed to investigation, validation of results, and reviewing/editing of the final work.

CC, MH, and SPW contributed to conceptualization, funding acquisition, project administration, resources, supervision, and reviewing/editing of the final work.

All authors read and approved the final manuscript.

Declarations

Conflicts of interest

There are no conflicts to declare.

Data availability

Data generated or analyzed during this study are included in this published article and its supplementary files. RNA sequencing data can be found in the SRA database at BioProject accession: PRJNA1347467.

Acknowledgments

This work was supported by the National Institutes of Health (Award No. **R21GM154180, 1R01CA286786**); the National Science Foundation (Award No. CBET **2232658**); the Eunice Kennedy Shriver National Institute of Child Health & Human Development of the National Institutes of Health (Award No. **T32HD087166),** MSU AgBio Research, and Michigan State University**.** Microscopy data was collected at the MSU Center for Advanced Microscopy. We also acknowledge the genomics services performed in the MSU Research Technology Support Facility Genomics Core as well as the RNA sequencing analyses performed by Dr. Nanye Long at the Michigan State University Bioinformatics Core (RRID:SCR_026706). The content is solely the responsibility of the

View Article Online
DOI: 10.1039/D6NR01765G

authors and does not necessarily represent the official views of the National Institutes of Health or the National Science Foundation.

View Article Online
DOI: 10.1039/D6NR01765G

References

1 S. Chen, Q. Bao, W. Xu and X. Zhai, *J Nanobiotechnol*, 2025, **23**, 263.
2 E. R. Abels and X. O. Breakefield, *Cell Mol Neurobiol*, 2016, **36**, 301–312.
3 L. Alvarez-Erviti, Y. Seow, H. Yin, C. Betts, S. Lakhal and M. J. A. Wood, *Nat Biotechnol*, 2011, **29**, 341–345.
4 Y. Liang, X. Xu, X. Li, J. Xiong, B. Li, L. Duan, D. Wang and J. Xia, *ACS Appl. Mater. Interfaces*, 2020, **12**, 36938–36947.
5 Y. Zhang, L. Li, J. Yu, D. Zhu, Y. Zhang, X. Li, H. Gu, C.-Y. Zhang and K. Zen, *Biomaterials*, 2014, **35**, 4390–4400.
6 Q. Zhang, J. N. Higginbotham, D. K. Jeppesen, Y.-P. Yang, W. Li, E. T. McKinley, R. Graves-Deal, J. Ping, C. M. Britain, K. A. Dorsett, C. L. Hartman, D. A. Ford, R. M. Allen, K. C. Vickers, Q. Liu, J. L. Franklin, S. L. Bellis and R. J. Coffey, *Cell Reports*, 2019, **27**, 940-954.e6.
7 Q. Zhang, D. K. Jeppesen, J. N. Higginbotham, R. Graves-Deal, V. Q. Trinh, M. A. Ramirez, Y. Sohn, A. C. Neininger, N. Taneja, E. T. McKinley, H. Niitsu, Z. Cao, R. Evans, S. E. Glass, K. C. Ray, W. H. Fissell, S. Hill, K. L. Rose, W. J. Huh, M. K. Washington, G. D. Ayers, D. T. Burnette, S. Sharma, L. H. Rome, J. L. Franklin, Y. A. Lee, Q. Liu and R. J. Coffey, *Nat Cell Biol*, 2021, **23**, 1240–1254.
8 S. Noguchi, S. Tozawa, T. Sakurai, A. Ohkuchi, H. Takahashi, H. Fujiwara and T. Takizawa, *Journal of Reproductive Immunology*, 2024, **161**, 104187.
9 H. Zhang, D. Freitas, H. S. Kim, K. Fabijanic, Z. Li, H. Chen, M. T. Mark, H. Molina, A. B. Martin, L. Bojmar, J. Fang, S. Rampersaud, A. Hoshino, I. Matei, C. M. Kenific, M. Nakajima, A. P. Mutvei, P. Sansone, W. Buehring, H. Wang, J. P. Jimenez, L. Cohen-Gould, N. Paknejad, M. Brendel, K. Manova-Todorova, A. Magalhães, J. A. Ferreira, H. Osório, A. M. Silva, A. Massey, J. R. Cubillos-Ruiz, G. Galletti, P. Giannakakou, A. M. Cuervo, J. Blenis, R. Schwartz, M. S. Brady, H. Peinado, J. Bromberg, H. Matsui, C. A. Reis and D. Lyden, *Nat Cell Biol*, 2018, **20**, 332–343.
10 J. D. Arroyo, J. R. Chevillet, E. M. Kroh, I. K. Ruf, C. C. Pritchard, D. F. Gibson, P. S. Mitchell, C. F. Bennett, E. L. Pogosova-Agadjanyan, D. L. Stirewalt, J. F. Tait and M. Tewari, *Proc. Natl. Acad. Sci. U.S.A.*, 2011, **108**, 5003–5008.
11 E. Willms, C. Cabañas, I. Mäger, M. J. A. Wood and P. Vader, *Front. Immunol.*, 2018, **9**, 738.
12 Q. Zhang, D. K. Jeppesen, J. N. Higginbotham, J. L. Franklin and R. J. Coffey, *Nat Protoc*, 2023, **18**, 1462–1487.
13 R. Štukelj, K. Schara, A. Bedina - Zavec, V. Šuštar, M. Pajnič, L. Pađen, J. L. Krek, V. Kralj-Iglič, A. Mrvar-Brečko and R. Janša, *European Journal of Pharmaceutical Sciences*, 2017, **98**, 17–29.
14 O. S. Tutanov, C. Massick, M. Ramirez, J. N. Higginbotham, L. Jimenez, M. Castleberry, Z. Cao, E. John, M. S. Hamilton, Q. Zhang, D. K. Jeppesen, D. L. Michell, S. E. Glass, P. Patel, K. L. Rose, E. Krystofiak, H.-C. Chen, Q. Sheng, Q. Liu, J. G. Patton, A. M. Weaver, J. L. Franklin, K. C. Vickers and R. J. Coffey, *Cell Reports*, 2025, **44**, 116287.
15 H. G. Pontis, in *Methods for Analysis of Carbohydrate Metabolism in Photosynthetic Organisms*, Elsevier, 2017, pp. 45–63.
16 G. Brusotti, E. Calleri, R. Colombo, G. Massolini, F. Rinaldi and C. Temporini, *Chromatographia*, 2018, **81**, 3–23.
17 M. Hall, in *Biopharmaceutical Processing*, Elsevier, 2018, pp. 421–432.
18 P. Agrawal, K. Wilkstein, E. Guinn, M. Mason, C. I. Serrano Martinez and J. Saylae, *Org. Process Res. Dev.*, 2023, **27**, 571–591.
19 S. Busatto, G. Vilanilam, T. Ticer, W.-L. Lin, D. Dickson, S. Shapiro, P. Bergese and J. Wolfram, *Cells*, 2018, **7**, 273.
20 Y. Kawai-Harada, V. Nimmagadda and M. Harada, *BMC Methods*, 2024, **1**, 9.
21 H.-W. Liu, Y. Hu, Y. Ren, H. Nam, J. L. Santos, S. Ng, L. Gong, M. Brummet, C. A. Carrington, C. G. Ullman, M. G. Pomper, I. Minn and H.-Q. Mao, *ACS Appl. Mater. Interfaces*, 2021, **13**, 30326–30336.

View Article Online
DOI: 10.1039/D6NR01765G

22 S. Higuchi, T. Satou and Y. Uchida, *MethodsX*, 2023, **10**, 102126.
23 D. C. Watson, B. C. Yung, C. Bergamaschi, B. Chowdhury, J. Bear, D. Stellas, A. Morales‐Kastresana, J. C. Jones, B. K. Felber, X. Chen and G. N. Pavlakis, *J of Extracellular Vesicle*, 2018, **7**, 1442088.
24 D. M. Berrie, R. C. Waters, C. Montoya, A. Chatel and E. M. Vela, *Vaccine*, 2020, **38**, 3639–3645.
25 M. Li, R. Soder, S. Abhyankar, T. Home, H. Pathak, X. Shen, A. K. Godwin and H. Abdelhakim, *Cytotherapy*, 2025, **27**, 1219–1228.
26 X.-C. Liu, J.-W. Tian, J.-Y. Xu, L.-G. Chen, Z.-W. Ye, J. Huang, L.-Z. Wu, Z.-L. Zhang, Z.-L. Yu and G. Chen, *Trends in Biotechnology*, 2025, **43**, 2947–2969.
27 M. Armstrong, L. Wang, K. Ristroph, C. Tian, J. Yang, L. Ma, S. Panmai, D. Zhang, K. Nagapudi and R. K. Prud'homme, *Journal of Pharmaceutical Sciences*, 2023, **112**, 2267–2275.
28 X. Osteikoetxea, B. Sódar, A. Németh, K. Szabó-Taylor, K. Pálóczi, K. V. Vukman, V. Tamási, A. Balogh, Á. Kittel, É. Pállinger and E. I. Buzás, *Org. Biomol. Chem.*, 2015, **13**, 9775–9782.
29 J. M. G. Artigas, M. E. Garcia, M. R. A. Faure and A. M. B. Gimeno, *Postgraduate Medical Journal*, 1981, **57**, 219–222.
30 J. C. Houck and L. B. Berman, *Journal of Applied Physiology*, 1958, **12**, 473–476.
31 M. Martin, *EMBnet j.*, 2011, **17**, 10.
32 A. Kozomara, M. Birgaoanu and S. Griffiths-Jones, *Nucleic Acids Research*, 2019, **47**, D155–D162.
33 M. R. Friedländer, S. D. Mackowiak, N. Li, W. Chen and N. Rajewsky, *Nucleic Acids Research*, 2012, **40**, 37–52.
34 M. I. Love, W. Huber and S. Anders, *Genome Biol*, 2014, **15**, 550.
35 J. Ren, Z. Li and F.-S. Wong, *Journal of Membrane Science*, 2006, **279**, 558–569.
36 S. Iwasaki, M. Kobayashi, M. Yoda, Y. Sakaguchi, S. Katsuma, T. Suzuki and Y. Tomari, *Molecular Cell*, 2010, **39**, 292–299.
37 J. M. Pare, N. Tahbaz, J. López-Orozco, P. LaPointe, P. Lasko and T. C. Hobman, *MBoC*, 2009, **20**, 3273–3284.
38 S. A. Müller, T. Sasaki, P. Bork, B. Wolpensinger, T. Schulthess, R. Timpl, A. Engel and J. Engel, *Journal of Molecular Biology*, 1999, **291**, 801–813.
39 V. Mussack, S. Hermann, D. Buschmann, B. Kirchner and M. W. Pfaffl, in *Quantitative Real-Time PCR*, eds. R. Biassoni and A. Raso, Springer New York, New York, NY, 2020, vol. 2065, pp. 23–38.
40 M. J. Rogers, A. Andreosso, J. Billakanti, M. G. Duke, Y. Lu, N. Collinson, J. Tan, L. Macia, N. Koifman, M. Floetenmeyer, M. K. Jones, C. A. Gordon and S. Navarro, 2025, preprint, DOI: 10.1101/2025.03.24.645107.
41 J. Morales-Sanfrutos, J. Etxeberria-Ugartemendia, O. Barroso-Gomila, E. González, M. Sendino, P. Ximénez-Embún, F. García, E. Zarzuela, J. M. Falcón-Pérez, H. Peinado and J. Muñoz, *Nat Cell Biol*, 2026, **28**, 622–639.
42 S. B. delCardayre and R. T. Raines, *Biochemistry*, 1994, **33**, 6031–6037.
43 B. M. Fisher, J. E. Grilley and R. T. Raines, *Journal of Biological Chemistry*, 1998, **273**, 34134–34138.
44 T. Cui, E. H. Bell, J. McElroy, A. P. Becker, P. M. Gulati, M. Geurts, N. Mladkova, A. Gray, K. Liu, L. Yang, Z. Liu, J. L. Fleming, S. J. Haque, J. S. Barnholtz-Sloan, K. L. Ligon, R. Beroukhim, P. Robe and A. Chakravarti, *Oncogene*, 2019, **38**, 2923–2936.
45 T. I.-S. Hwang, P.-C. Chen, T.-F. Tsai, J.-F. Lin, K.-Y. Chou, C.-Y. Ho, H.-E. Chen and A.-C. Chang, *Cell Death Dis*, 2022, **13**, 390.
46 X. Wang, *Bioinformatics*, 2014, **30**, 1377–1383.
47 S. W. Eichhorn, H. Guo, S. E. McGeary, R. A. Rodriguez-Mias, C. Shin, D. Baek, S. Hsu, K. Ghoshal, J. Villén and D. P. Bartel, *Molecular Cell*, 2014, **56**, 104–115.
48 C. Villarroya-Beltri, C. Gutiérrez-Vázquez, F. Sánchez-Cabo, D. Pérez-Hernández, J. Vázquez, N. Martin-Cofreces, D. J. Martinez-Herrera, A. Pascual-Montano, M. Mittelbrunn and F. Sánchez-Madrid, *Nat Commun*, 2013, **4**, 2980.

View Article Online
DOI: 10.1039/D6NR01765G

49 A. J. McKenzie, D. Hoshino, N. H. Hong, D. J. Cha, J. L. Franklin, R. J. Coffey, J. G. Patton and A. M. Weaver, *Cell Reports*, 2016, **15**, 978–987.
50 C. Booyjżsen, C. A. Scarff, B. Moreton, I. Portman, J. H. Scrivens, G. Costantini and P. J. Sadler, *Biochimica et Biophysica Acta (BBA) - General Subjects*, 2012, **1820**, 427–436.
51 L. Zhang, J. Song, G. Cavigiolio, B. Y. Ishida, S. Zhang, J. P. Kane, K. H. Weisgraber, M. N. Oda, K.-A. Rye, H. J. Pownall and G. Ren, *Journal of Lipid Research*, 2011, **52**, 175–184.
52 M. Uhlén, L. Fagerberg, B. M. Hallström, C. Lindskog, P. Oksvold, A. Mardinoglu, Å. Sivertsson, C. Kampf, E. Sjöstedt, A. Asplund, I. Olsson, K. Edlund, E. Lundberg, S. Navani, C. A.-K. Szigyarto, J. Odeberg, D. Djureinovic, J. O. Takanen, S. Hober, T. Alm, P.-H. Edqvist, H. Berling, H. Tegel, J. Mulder, J. Rockberg, P. Nilsson, J. M. Schwenk, M. Hamsten, K. Von Feilitzen, M. Forsberg, L. Persson, F. Johansson, M. Zwahlen, G. Von Heijne, J. Nielsen and F. Pontén, *Science*, 2015, **347**, 1260419.
53 The Human Protein Atlas, proteinatlas.org.
54 C. E. Condrat, D. C. Thompson, M. G. Barbu, O. L. Bugnar, A. Boboc, D. Cretoiu, N. Suciu, S. M. Cretoiu and S. C. Voinea, *Cells*, 2020, **9**, 276.
55 W. Sakamoto, T. Masuno, H. Yokota and T. Takizawa, *Molecular Medicine Reports*, 2017, **15**, 1989–1996.
56 I. S. Pires and A. F. Palmer, *Journal of Membrane Science*, 2021, **618**, 118712.

View Article Online
DOI: 10.1039/D6NR01765G

Data availability statement

Data generated or analyzed during this study are included in this published article and its supplementary files. RNA sequencing data can be found in the SRA database at BioProject accession: PRJNA1347467.